Ocean Sci. Discuss., 9, 2535–2559, 2012
www.ocean-sci-discuss.net/9/2535/2012/
doi:10.5194/osd-9-2535-2012

Ocean Science Discussions

Impact of the sea surface temperature forcing on hindcasts of Madden-Julian Oscillation events using the ECMWF model

E. de Boisséson[1,2], **M. A. Balmaseda**[2], **F. Vitart**[2], **and K. Mogensen**[2]

[1]CNRM/GAME, URA 1357, 42 avenue Gaspard Coriolis, 31057, Toulouse, France
[2]European Centre for Medium Range Forecast, Shinfield Park, RG2 9AX, Reading, UK

Received: 29 June 2012 – Accepted: 4 July 2012 – Published: 23 July 2012

Correspondence to: E. de Boisséson (ne9@ecmwf.int)

Published by Copernicus Publications on behalf of the European Geosciences Union.

Abstract

This paper explores the sensitivity of the prediction of Madden Julian Oscillation (MJO) events to different aspects of the sea surface temperature (SST) in the European Centre for Medium-range Weather Forecasts (ECMWF) model. The impact of temporal resolution of SST on the MJO is first evaluated via a set of monthly hindcast experiments. The experiments are conducted with an atmosphere forced by persisted SST anomalies, monthly and weekly SSTs. Skill scores are clearly degraded when weekly SSTs are replaced by monthly values or persisted anomalies. The new high resolution OSTIA SST daily reanalysis would in principle allow to establish the impact of daily versus weekly SST values on the MJO prediction. It is found however that OSTIA SSTs provide lower skill scores than the weekly product. Further experiments show that this loss of skill cannot be attributed to either the mean state or the daily frequency of OSTIA SSTs. Additional diagnostics show that the phase relationship between OSTIA SSTs and tropical convection is not optimal with repspect to observations. Such result suggests that capturing the correct SST-convection phase relationship is a major challenge for the MJO predictions.

1 Introduction

The Madden-Julian Oscillation (MJO) is the major mode of intraseasonal variability (ISV) in the tropical atmosphere (Zhang, 2005). It is characterized by an Eastward propagation of regions of both enhanced and suppressed convection, mainly observed over the Indian and the Pacific Oceans. The MJO is known to influence the Asian (e.g. Murakami, 1976; Yasunari, 1979) and Australian monsoon (Hendon and Liebmann, 1990), the evolution El Nino events (e.g. Kessler and McPhaden, 1995) and the weather regimes over the North Atlantic European region in winter (Cassou, 2008; Vitart et al., 2010). The simulation and the predicatibility of such intraseasonal and seasonal weather regimes need an accurate representation of the MJO in the General

OSD
9, 2535–2559, 2012

Circulation Models (GCM). While simulating the MJO used to be diffcult in term of propagation of the convective centre (Slingo et al., 1996) and of the intensity of the associated ISV (Lin et al., 2006), new-generation models are now able to reproduce a realistic MJO (Lin et al., 2008; Vitart et al., 2010). Because of its importance for the predictability at intraseasonal and seasonal time scales, the MJO is one of the main benchmarks for the skill of the extended-range forecast systems.

Using a previous cycle of the Integrated Forecast System (IFS) of the European Center for Medium-range Weather Forecasts (ECMWF), Woolnough et al. (2007) showed that ocean/atmosphere coupled predictions of the MJO were superior to predictions produced by persisting the SST. They suggest that the simulation of the MJO needs accurate air-sea interactions through a good representation of the ISV and of the diurnal cycle of the SST. By focusing on the representation of the MJO in the Seoul National University atmospheric GCM, Kim et al. (2008) showed that high temporal SST frequency improved the simulation of the atmospheric ISV, of the propagation of the MJO and increased the MJO forecast skill. Kim et al. (2008) also argued that the simulation of the MJO needs a good representation of the phase relationship between SST and convection as provided in coupled general circulation model.

In recent years the increase of number of satellite instruments has enhanced the developement of SST analysis products, such as those from the Group for High-Resolution Sea Surface Temperature (GHRSST, see Donlon et al., 2007, http://www.ghrsst-pp.org/). Among these products is the recent 1/4° daily OSTIA (Operational Sea Surface Temperature and Sea-Ice Analysis) SST reanalysis (Roberts-Jones et al., 2011), which uses both satellite and in-situ data and spans the period January 1985–December 2007. The potential impact of such SST reanalysis in extended-range hindcast and atmosphereic reanalysis activities has to be assessed. For instance, the latest ECMWF ERA interim atmospheric reanalysis (Dee et al., 2011) uses SST from different sources according to the considered period: the 1 × 1° weekly NCEP 2d-var reanalysis from January 1981 to June 2001 (Reynolds et al., 2002), the 1 × 1° weekly NCEP OIv2 SST reanalysis from July 2001 to December 2001 (Reynolds et al., 2002), the daily 1/2°

OSD
9, 2535–2559, 2012

Real Time Global (RTG) SST analysis from January 2002 to January 2009 (Gemmill et al., 2007) and the 1/20° daily OSTIA from February 2009 onwards (Donlon et al., 2011). Before 1981 and the satellite era, the ECMWF reanalyses use the HADISST1 dataset of monthly SST values produced by the Met Office (Rayner et al., 2003).

This work is an attempt to assess the impact of different kinds of SST forcings on the prediction of past MJO events in atmosphere-only mode using a recent cycle of the IFS. The winter 1992/1993 MJO is used as benchmark case at ECMWF as in Woolnough et al. (2007). First the impact of the temporal resolution of SST on the MJO prediction is investigated. The skill of the IFS in predicting the 1992–1993 MJO is assessed for different SST fields: persisted SST anomalies, weekly observed SST used in ERA interim, monthly ERA interim SST (to simulate the pre-sattelite era), daily OSTIA SST reanalysis. Then this study particularly insists on the experiments using the current ECMWF observed SST and the OSTIA reanalysis to highlight the sensitivity of the intra-seasonal prediction to "realistic" SST forcing. In the following, Sect. 2 describes the experiment settings, the SST products and the resulting MJO scores. Section 3 focuses on the difference between the forecast using OSTIA SST and observed SST from ERA interim. Section 4 discusses the outcomes of the experiments and Sect. 5 draws the conclusions of this study.

2 MJO experiments

2.1 Experiment settings

The experimental settings for the MJO forecast are similar to the ones described in Woolnough et al. (2007). Each experiment consists of a series of 32-day forecasts using a five-member ensemble initialized at 00:00 UTC each day from 15 December 1992 to 31 January 1993. In our experiments, the atmospheric component of the monthly forecasting system is the Integrated Forecasting System (IFS) cycle 36R4. The horizontal resolution is T_L159 with 62 vertical levels. The atmospheric initial conditions

OSD
9, 2535–2559, 2012

come from the ERA interim reanalysis (Dee et al., 2011). A skin layer scheme has been implemented in the IFS to simulate the diurnal variations of SST (see Zeng and Beljaars, 2005; Takaya et al., 2010). Four MJO experiments (see Table 1) are conducted in atmosphere-only mode where the atmosphere is forced by: (i) persisted SST anomalies (perSSTa), (ii) SST from ERA interim (ERAi), (iii) monthly SST (MTH) and (iv) OSTIA SST. These SSTs corresponds to the foundation SST defined by the GHRSST as the temperature at the base of the diurnal thermocline.

2.2 SST products

Persisted SST anomalies are obtained by adding ERA interim SST anomalies (against the climatology) of the starting date to the SST climatology corresponding to the forecast lead time. For the 1992–1993 time period, ERA interim SSTs (referred to as ERAi SST) come from the NCEP 2Dvar SST, originally a weekly $1^{\circ} \times 1^{\circ}$ analysis (Reynolds et al., 2002) available from 1981. This analysis combines the information from in situ data (from ships and buoys) and from the Advanced Very High Resolution Radiometer (AVHRR) satellite. Weekly SSTs are then daily interpolated according to the forecast lead time. The ERAi SSTs are consistent with the initial atmospheric conditions of the MJO experiment. Monthly SSTs are obtained by applying a 30-day running mean to the ERAi SST fields. OSTIA SSTs come from the daily $1/4^{\circ}$ OSTIA reanalysis (Roberts-Jones et al., 2011), which is independent of ERA interim. This analysis combines the information from in situ data (from ships and buoys), from the AVHRR satellite and from the Along Track Scanning Radiometer (ATSR) instruments on board of the ERS-1, ERS-2 and ENVISAT satellites.

2.3 Diagnostic procedure

The skill of the monthly forecasting system in predicting the MJO is evaluated according to the method described in Wheeler and Hendon (2004). This method considers that the ISV of the MJO can be captured by a combined Empirical Orthogonal Function

OSD
9, 2535–2559, 2012

(EOF) analysis of the anomalies (with respect to the 1991–2003 climate) of the zonal wind at 200 hPa and 850 hPa and of the outgoing longwave radiation (OLR) averaged between 10° S and 10° N. Wheeler and Hendon (2004) showed that most of the MJO variability is described by the two first components of the combined EOF analysis. Their longitudinal patterns can represent all the active and suppressed phases of the MJO (Fig. 1) over its eastward propagation. Negative OLR extrema reflect the position of the convective centre of the MJO. According to the sign of the associated Principal Component (PC), the convective centre on EOF1 is located over the Maritime Continent (PC1 > 0) or over the Western Hemisphere and Africa (PC1 < 0). On EOF2, the convection is over the Pacific Ocean (PC2 > 0) or over the Indian Ocean (PC2 < 0). The recommended score of the MJO forecast relies on the correlation of the monthly ensemble-mean forecasts with the two first PCs of the combined EOFs estimated from the ERA interim atmospheric reanalysis. According to Woolnough et al. (2007), two MJO events occur between mid-December 1992 and February 1993. The 47 starting dates of the experiments include all the phases of these MJO events as identified by the combined EOF analysis. Plus, each forecast captures each phase of the MJO at least once.

3 Results and outcomes

3.1 Results

The correlations of the ensemble-mean forecast with the two principal components of the combined EOF are estimated for all the experiments (Fig. 2). The forecast skill is considered as significant for correlations higher than 0.6. Both correlations show that the ERAi and OSTIA experiments have overall better forecast skill than perSSTa. These three experiments show correlations higher than 0.9 until day 8 of the forecast on EOF1 and day 14 on EOF2. Then the correlations begin to diverge and, at the significance level, the ERAi and OSTIA scores are beyond day 22 while perSSTa only reach day

OSD
9, 2535–2559, 2012

18 implying a gain of at least 4 days of MJO forecast skill on both EOFs. Such gain was expected considering that ERAi and OSTIA SST – being real-time observed fields – have an ISV signal that is closer to the truth than the climatological signal of the persisted SST anomalies. Another expected result is the degradation of the forecast when using monthly SST. The MTH experiment scores are sometimes even worse than perSSTa and, when comparing to ERAi and OSTIA, they show a loss of significant forecast skill of at least 3 to 5 days on EOF 1 and 2, respectively. Such performance has to be expected when reforecasting similar MJO events before 1981 (pre-satellite era). ERAi and OSTIA are the two best experiments. Their scores are similar until day 16 on EOF1 and 18 on EOF2, then ERAi provides a gain of one day of significant skill on EOF1 and at least more than 3 on EOF2. Forcing with weekly ERAi SSTs is better at predicting the MJO of the winter 1992–1993 than forcing with daily OSTIA SSTs. This result is unexpected because, according to Kim et al. (2008) and Klingaman et al. (2008), the daily frenquency should have a positive impact on the representation of the tropical ISV and thus on the forecast of the MJO.

3.2 Outcomes

As providing higher ISV to the atmosphere seems to improve significantly the MJO prediction in the case of the ERAi and OSTIA experiments, one can think of an alternative to forcing by persisted SST anomalies or monthly SSTs. According to works from Woolnough et al. (2007) and Vitart et al. (2007) coupling the atmosphere to the ocean would be a good candidate in the case of the extended range forecast or from the reanalysis point of view. Addressing these aspects is nevertheless beyond the scope of our study.

More interesting is the fact that forcing with weekly ERAi SSTs provides better MJO prediction than forcing with daily OSTIA SSTs. To visualise how the two forced experiments differ, the propagation of the MJO signal in the forecasts is tracked in longitudinal hovmoller diagrams of the ensemble-mean OLR anomalies averaged between 10° S and 10° N. In Fig. 3, the forecasts and their equivalent in the ERA interim analysis are

OSD
9, 2535–2559, 2012

averaged for starting dates when the convective centre of the MJO is over the Indian Ocean. In the analysis, the convective centre of the MJO (negative OLR anomalies) propagates from the Indian to the Central Pacific Ocean and is followed by a phase of suppressed convection (positive OLR anomalies) a few days later. The ERAi experiment simulates correctly this propagation but the MJO active and suppressed phases are much weaker than in the analysis. The weakening is particarly marked when the convection reaches the Maritime Contient that is known as a barrier for the MJO simulation (Inness et al., 2003). In the OSTIA experiment, the MJO signal is even weaker over the Maritime Continent and its eastern propagation is hardly visible. The difference between the ERAi and OSTIA experiment only comes from the SSTs forcing the atmosphere. The relative impact of these two SST fields on the MJO prediction is investigated in the next sections.

4 Origins of the difference in the forecasts using OSTIA and ERAi SSTs

4.1 OSTIA versus ERAi SSTs: mean state and daily variability

Apart from the horizontal resolution of the source fields (before the interpolation on the atmospheric grid), the main differences between OSTIA and ERAi SSTs come from their mean state and the additional noise associated to the daily frequency of the OSTIA product. On average over the winter 1992–1993, the OSTIA SSTs are overall colder than ERAi SSTs by 0.18 °C in the Tropics. Apart from some warmer patches, OSTIA SSTs are particularly colder (sometimes by more than 0.4 °C) in the western part of the Maritime Continent, in the Pacific cold tongue and in the Tropical Atlantic (Fig. 4). At the TAO station 2° S–156° E, the OSTIA product seems overall closer to the in situ observations than ERAi SST over the winter 1992–1993. With respect with ERAi SST, OSTIA SSTs show more variance than ERAi SSTs (0.76 versus 0.9), which is closer to the observations (variance of 0.17). OSTIA SSTs also show a better correlation (0.9 versus 0.16) and a lower root mean square error (0.21 versus 0.27). Such

OSD
9, 2535–2559, 2012

agreement is not observed at every TAO station but supports the accuracy of the OSTIA product.

4.2 OSTIA versus ERAi SSTs: phase relationship between SST and convection

This section investigates the difference in the phase relationship between SST and atmospheric convection. This phase realtionship is estimated in the Indian Ocean over the winters (December–February) 1985–2006: from ERAi and OSTIA SSTs fields and OLR (indicative of the convection) from the ERA interim reanalysis and from National Oceanic and Atmospheric Administration (NOAA) daily interpolated OLR (see Liebmann and Smith, 1996). The NOAA interpolated OLR is produced from the NOAA satellite retrievals on a 2.5° × 2.5° grid and is available from 1979 onwards. The phase relationship between SST and convection is produced from filtered SST and OLR anomalies averaged in the Indian Ocean box 5° S–5° N, 60°–95° E with respect with their respective 1985–2006 mean. Following the method of Kim et al. (2008), for each date, the interannual variability of SST and OLR is removed by substracting their respective 30-day mean (the 30 days following the considered date). The intraseasonal variability is then extracted from SST and OLR by applying a 5-day running mean. The resulting lag-correlation between SST and OLR shows a near-quadrature phase relationship (Fig. 5): positive OLR anomalies (suppressed convection) lead enhanced SST anomalies, and negative OLR anomalies (enhanced convection) lag enhanced SST anomalies after several days. When using ERAi SST and NOAA OLR, the extremum correlations occur at lag −10 days (0.45) and +12 days (−0.38). The phase relationship in ERA interim (ERAi SST and OLR) is similar in shape but with slightly smaller amplitude: 0.39 and −0.37. When using OSTIA SST with either NOAA or ERA interim OLR, the phase relationship is shifted by almost 3 days toward the negative lags. The amplitude of the relationship is also weaker than with ERAi SST (extremum correlations around 0.27 and −0.21). This result suggests that the relationship between SST and the current atmospheric products on intraseasonal time-scale is weaker when using OSTIA SST than when using ERAi SST.

OSD
9, 2535–2559, 2012

4.3 Impact of the mean state and the daily variability on the MJO prediction

From the MJO point of view, OSTIA SSTs – being colder than ERAi SSTs – should be less prone to trigger convection and to propagate the MJO signal. Similarly, if the daily variability introduced by the OSTIA SSTs is not in phase with the amospheric model, one expects a distortion and the destruction of the convection associated to the MJO. In that respect, the weekly variablity of ERAi SST fields should have less negative impact on the simulation of the MJO. To assess the impact of the mean state and of the time variability in the OSTIA product, two additional experiment have been conducted. First, the mean state of OSTIA SST is corrected in each forecast by removing the averaged difference between OSTIA SST and ERAi SST over the forecast length. Second, the daily variability in OSTIA is smoothed by applying a weekly running mean on the OSTIA SST fields. The scores of these two MJO experiments (Fig. 6) show little or no improvement compared to the forcing by raw OSTIA SSTs for the two EOFs suggesting that neither the mean state nor the daily variability of OSTIA SST are one of the main reasons of the deterioration (with respect to the forcing by ERAi SST) of the MJO prediction.

4.4 Representativity of the winter 1992–1993 MJO case: 22 winter experiments

To investigate the representativity of the differences between the experiments performed with OSTIA and ERAi SSTs over the winter 1992–1993, similar experiments are conducted over 22 winters (from December to February) from 1985 to 2006. As mentioned in the Introduction, over 1985–2006, ERAi SSTs are produced from the $1 \times 1^{\circ}$ weekly NCEP 2d-var reanalysis from January 1981 to June 2001, the $1 \times 1^{\circ}$ weekly NCEP OIv2 SST reanalysis from July 2001 to December 2001 and the daily $1/2^{\circ}$ RTG SST analysis from January 2002. The two new ERAi and OSTIA expiments include 5 forecasts per winter, every 15 days from 1 December to 1 February. The configuration is the same as for previous experiments (see Sect. 2.1). The resulting scores of the ERAi and OSTIA experiments for the MJO forecast show significant skill only up

OSD
9, 2535–2559, 2012

to 19 days for PC1 and 16 days for PC2, which is substantially less than the 20 days and more obtained for the only 1992–1993 case. The difference between the ERAi and OSTIA experiments is weaker than for the 1992–1993 case with rarely more than 1 day of loss of forecast skill when using OSTIA SST instead of ERAi SST. The scores nevertheless confirm that forcing the atmopshere by OSTIA SST is less efficient than forcing by ERAi SST (Fig. 7) in predicting the MJO.

4.5 Phase relationship between SST and convection in the experiments

The 22-winter experiments provide enough data to investigate the phase relationship between the OSTIA and ERAi SST and the atmospheric convection (OLR) according to the forecast lead time. This relationship is estimated in a similar way as in Sect. 4.2. The interannual variability in each 32-day forecast is removed by substracting its 32-day mean. The intraseasonal variability is then extracted by applying a 5-day running mean in each forecast segment. The evolution of the phase relationship between the SST and OLR in the Indian Ocean (5° S–5° N, 60°–95° E) according to the lead time in the two forced experiments is compared to the equivalent in the ERA interim analysis. As seen in Sect. 4.2 (Fig. 5), the analysis shows a near-quadrature phase relationship (Fig. 8). Extremum correlations occur around 7–10 days according to the considered forecast week. Both the forecast forced by OSTIA SST and ERAi SST produce similar phase relationships that are, though sometimes weakened, overall close to the analysis until week 3 of the forecast. The forecast forced by OSTIA is nevertheless slightly shifted toward negative lags in week 1 of the forecast. The phase relationship is recovered in weeks 2 and 3 but with lower correlations than in the ERAi experiment when the lag is negative. The OSTIA experiment loses the quadrature phase relationship in week 4 of the forecast while the ERAi experiment keeps some consistency with the analysis. This diagnostics is consistent with what is shown in Sect. 4.2 and suggests that forcing by OSTIA SST relatively degrades the phase relationship between SST and convection. This degradation implies less efficiency to maintain and propagate the MJO signal when OSTIA SSTs are used to force the atmospheric model.

OSD
9, 2535–2559, 2012

5 Discussion and conclusion

This study suggests that the relative loss of MJO forecast skill when forcing with OSTIA SST is related to an inaccury in the phase relationship between OSTIA SST and the atmospheric convection produced in the model (Fig. 8). A similar inaccuracy has also been reported between OSTIA SST and the convection derived from satellite observations (Fig. 5). From the initial state of the MJO prediction using OSTIA SST, the atmosphere and its lower boundary conditions are not as consistent as they are when using ERAi SST. This is most likely linked to the fact that the initial state of the atmospheric model comes from the ERA interim reanalysis that has been produced using the ERAi SSTs as boundary conditions for the atmospheric model. One can easily expect an initialization shock that would deteriorate the prediction. Moreover, the OSTIA SSTs here come from a 1/4° resolution product that is interpolated on the T159 atmospheric grid for the purpose of our experiments. Even smoothed by the interpolation, the resulting fields are spatially much noisier than ERAi SSTs. Noisy features may generate air-sea interactions weakening the MJO signal in a low resolution atmosphere starting from an initial state produced by using smooth ERAi SST fields. The Maritime Continent being a barrier to the MJO prediction, an initially weakened MJO signal will have difficulties to propagate over and past this barrier as described on Fig. 3 in the OSTIA experiment. A way to assess the potential importance of the initial bias of the atmosphere toward ERA interim, would be to produce a similar atmospheric reanalysis using OSTIA SSTs as boundary conditions over the period of the forecast. This reanalysis would then be used as initial states for the new experiments forced by OSTIA and ERAi SSTs.

This study assesses the impact of different kinds of SST forcings on the prediction of past MJO events in the atmosphere-only mode of the IFS. The focus has been put on the benchmark case of the MJO of the winter 1992–1993. The MJO experiments show that forcing the atmosphere by either persisted SST anomalies (like in the medium range forecast at ECMWF) or monthly SSTs (like in climate run or reanalysis prior to the satellite era) is not optimal. The experiments forced by weekly ERAi and

OSD
9, 2535–2559, 2012

daily OSTIA SSTs show that SSTs with accurate intraseasonal variability significantly improved the prediction. The MJO prediction shows substantial sensitivity to these two SST forcings. The prediction forced by OSTIA SST shows a loss of forecast skill of several days when compared to the prediction forced by ERAi SST. Sensitivity experiments show that this deterioration is linked neither to the difference in mean state between OSTIA and ERAi SSTs nor to the OSTIA daily variability. Additional diagnostics show that, the OSTIA product provides an anoumalously weak and shifted phase relationship on the intraseasonal time-scale between SST and convection from the beginning of the prediction. This phase relationship is never totally recovered, leading to the simulation of a weakened MJO signal with increased difficulties to propagate. Though close to in-situ SST observations, the consistency of the OSTIA product with the ECMWF atmospheric model is not optimal.

Acknowledgements. Eric de Boisseson is supported by CNRS-INSU and ECMWF. This is a contribution to the MyOcean project.

The publication of this article is financed by CNRS-INSU.

OSD
9, 2535–2559, 2012

References

Cassou, C.: Intraseasonal interaction between the Madden-Julian Oscillation and the North Atlantic Oscillation, Nature, 455, 523–527, 2008. 2536

Dee D. P., Uppala, S. M., Simmons, A. J., Berrisford, P., Poli, P., Kobayashi, S., Andrae, U., Balmaseda, M. A., Balsamo, G., Bauer, P., Bechtold, P., Beljaars, A. C. M., van de Berg, L., Bidlot, J., Bormann, N., Delsol, C., Dragani, R., Fuentes, M., Geer, A. J., Haimberger, L., Healy, S. B., Hersbach, H., Holm, E. V., Isaksen, L., Kallberg, P., Kohler, M., Matricardi, M., McNally, A. P., Monge-Sanz, B. M., Morcrette, J.-J., Park, B.-K., Peubey, C., de Rosnay, P., Tavolato, C., Thepaut, J.-N., and Vitart, F.: The ERA-Interim reanalysis: configuration and performance of the data assimilation system, Q. J. Roy. Meteorol. Soc. 137, 553–597, 2011. 2537, 2539

Donlon, C., Robinson, I., Casey, K., Vasquez, J., Armstrong, E., Gentemann, C., May, D., LeBorgne, P., Piollé, J., Barton, I., Beggs, H., Poulter, D. J. S., Merchant, C., Bingham, A., Heinz, S., Harris, A., Wick, G., Emery, B., Stuart-Menteth, A., Minnett, P., Evans, B., Llewellyn-Jones, D., Mutlow, C., Reynolds, R., Kawamura, H., and Rayner, N.: The global ocean data assimilation experiment high-resolution sea surface temperature pilot, B. Am. Meteor. Soc., 88, 1197–1213, 2007 2537

Donlon, C. J., Martin, M., Stark, J. D., Roberts-Jones, J., Fiedler, E., and Wimmer, W.: The Operational Sea Surface Temperature and Sea Ice analysis (OSTIA), Remote Sens. Environ., doi:10.1016/j.rse.2010.10.017, 2011. 2538

Gemmill W., Katz, B., and Li, X.: Daily, real-time, global sea surface temperature – high resolution analysis: RTG SST HR, NCEP/EMC Office Note, 39 pp., 2007. 2538

Hendon, H. H. and Liebmann, B.: A composite study of onset of the Australian summer monsoon, J. Atmos. Sci., 47, 2227–2240, 1990. 2536

Inness, P. M., Slingo, J. M., Guilyardi, E., and Cole, J.: Simulation of the Madden-Julian Oscillation in a coupled general circulation model, part II: the role of the basic state, J. Climate, 16, 365–382, 2003. 2542

Kessler, K. S. and McPhaden, M.: Oceanic equatorial waves and the 1991–93 El Niño, J. Climate, 8, 1757–1774, 1995. 2536

Kim, H. M., Hoyos, C. D., Webster, P. J., and Kang, I. S.: Sensitivity of MJO simulation and predictability to sea surface temperature variability, J. Climate, 21, 5304–5317, 2008. 2537, 2541, 2543

OSD
9, 2535–2559, 2012

Klingaman, N. P., Woolnough, S. J., Weller, H., and Slingo, J. M.: The importance of high-frequency sea surface temperature variability to the intraseasonal oscillation of Indian monsoon rainfall, J. Climate, 21, 6119–6140, 2011. 2541
Liebmann, B. and Smith, C. A.: Description of a complete (interpolated) outgoing longwave radiation dataset, B. Am. Meteorol. Soc., 77, 1275–1277, 1996. 2543
Lin, J. L., Kiladis, G. N., Mapes, B. E., Weickmann, K. M., Sperber, K. R., Lin, W., Wheeler, M., Schubert, S. D., Del Genio, A., Donner, L. J., Emori, S., Gueremy, J.-F., Hourdain, F., Rasch, P. J., Roeckner, E., and Scinocca, J. F.: Tropical intraseasonal variability in 14 IPCC AR4 climate models, part I: convective signals, J. Climate, 19, 2665–2690, 2006. 2537
Lin,. H., Brunet, G., and Derome, J.: Intraseasonal variability in a dry atmospheric model, J. Atmos. Sci., 28, 702–708, 2007.
Lin, H., Brunet, G., and Derome, J.: Forecast skill of the Madden-Julian Oscillation in two Canadian atmospheric models, Mon. Weather Rev., 136, 4130–4149, 2008. 2537
Mogensen, K. S., Balmaseda, M. A., and Weaver, A.: The NEMOVAR ocean data assimilation as implemented in the ECMWF ocean analysis for system 4, ECMWF Technical Memorandum No. 668, 2012.
Murakami, T.: Cloudiness fluctuations during the summer monsoon, J. Meteor. Soc. Jpn, 54, 175–181, 1976. 2536
Rayner, N. A., Parker, D. E., Horton, E. B., Folland, C. K., Alexander, L. V., Rowell, D. P., Kent, E. C., and Kaplan, A.: Global analyses of sea surface temperature, sea ice, and night marine air temperature since the late nineteenth century, J. Geophys. Res., 108, D144407, doi:10.1029/2002JD002670, 2003. 2538
Reynolds, R. W., Rayner, N. A., Smith, T. M., Stokes, D. C., and Wang, W.: An improved in situ and satellite SST analysis for climate, J. Climate, 15, 1609–1625, 2002. 2537, 2539
Roberts-Jones J., Fiedler, E., and Martin, M.: Description and Assessment of the OSTIA Reanalysis, UK MetOffice Forecasting Research, Technical Report No. 561, 2011. 2537, 2539
Slingo, J. M., Sperber, K. R., Boyle, J. S., Ceron, J.-P., Dix, M., Dugas, B., Ebisuzaki, W., Fyfe, J., Gregory, D., Gueremy, J.-F., Hack, J., Harzallah, A., Inness, P., Kitoh, A., Lau, W. K.-M., McAvnaey, B., Madden, R., Matthews, A., Palmer, T. N., Park, C.-K., Randall, D., and Renno, N.: Intraseasonal oscillations in 15 atmospheric general circulation models: results from an AMIP diagnostic subproject, Clim. Dynam., 12, 325–357, 1996. 2537

OSD
9, 2535–2559, 2012

Takaya, Y., Bidlot, J.-R., Beljaars, A. C. M., and Janssen, P. A. E. M.: Refinements to a prognostic scheme of skin sea surface temperature, J. Geophys. Res., 115, C06009, doi:10.1029/2009JC005985, 2010. 2539

Vitart, F., Woolnough, S. J., Balmaseda, M. A., and Tompkins, A. M.: Monthly forecast of the Madden-Julian Oscillation using a coupled GCM, Mon. Weather Rev., 135, 2700–2715, 2007. 2541

Vitart, F. and Molteni, F.: Simulation of the Madden-Julian Oscillation and its teleconnections in the ECMWF forecast system, Q. J. Roy. Meteorol. Soc., 136, 842–855, 2010. 2536, 2537

Wheeler, M. C. and Hendon, H. H.: An all-season real-time multivariate MJO index: development of an index for mMonitoring and prediction, Mon. Weather Rev., 132, 1917–1932, 2004. 2539, 2540, 2552

Woolnough, S. J., Vitart, F., and Balmaseda, M. A.: The role of the ocean in the Madden-Julian Oscillation: implications for MJO prediction, Q. J. Roy. Meteorol. Soc., 133, 117–128, 2007. 2537, 2538, 2540, 2541

Yasunari, T.: Cloudiness fluctuations associated with the Northern Hemisphere summer monsoon, J. Meteorol. Soc. Jpn, 57, 225–242, 1979. 2536

Zeng, X. and Beljaars, A.: A prognostic scheme of sea surface skin temperature for modeling and data assimilation, Geophys. Res. Lett., 32, L14605, doi:10.1029/2005GL023030, 2005. 2539

Zhang, C.: Madden-Julian Oscillation, Rev. Geophys., 43, RG2003, doi:10.1029/2004RG000158, 2005. 2536

OSD

9, 2535–2559, 2012

Table 1. Experiments performed with the ECMWF model in atmosphere-only mode and their respective SST forcing for the MJO case of the winter 1992–1993.

Experiment name	Nature of the SST forcing
perSSTa	persisted SST anomalies
ERAi	SST from the ERA interim reanalysis (ERAi SST)
MTH	monthly running mean of the ERAi SST
OSTIA	OSTIA SST reanalysis

OSD
9, 2535–2559, 2012

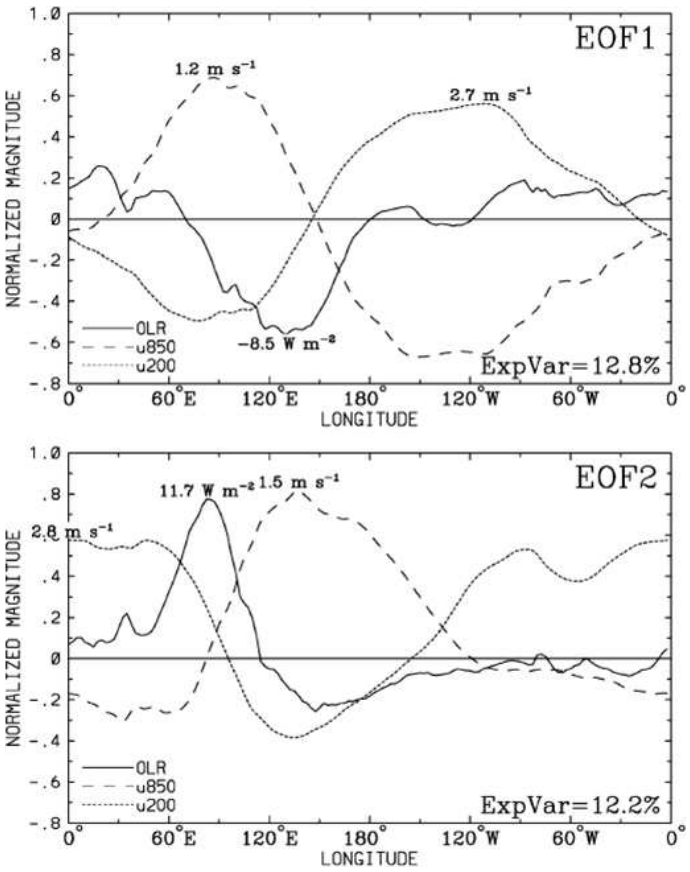

Fig. 1. Fig. 1 from Wheeler and Hendon (2004). Spatial structures of EOFs 1 and 2 of the combined analysis of anomalies of OLR, and of zonal wind (u) at 850, and 200 hPa. The variance explained by the respective EOFs is 12.8 % and 12.2 %

OSD
9, 2535–2559, 2012

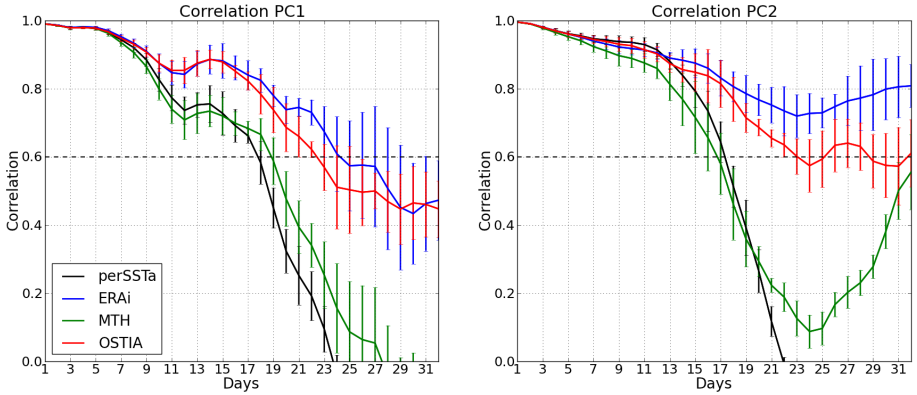

Fig. 2. Correlation of the PC1 (left) and PC2 (right) from the reanalysis with the ensemble mean forecast time series, based on 47 start dates (15 December 1992 to 31 January 1993), for the atmosphere-only experiments performed with the ECMWF forecast system at the T_L159 resolution. The atmosphere is forced from day 0 to 32 of the forecast by: persisted SST anomalies (perSSTa, black line), weekly ERAi SSTs (ERAi, blue line), monthly SSTs (MTH, green line), daily OSTIA SSTs (OSTIA, red line). The signifcance level (correlation of 0.6) is highlighted by a black dashed line. Error bars stand for the ensemble spread.

OSD
9, 2535–2559, 2012

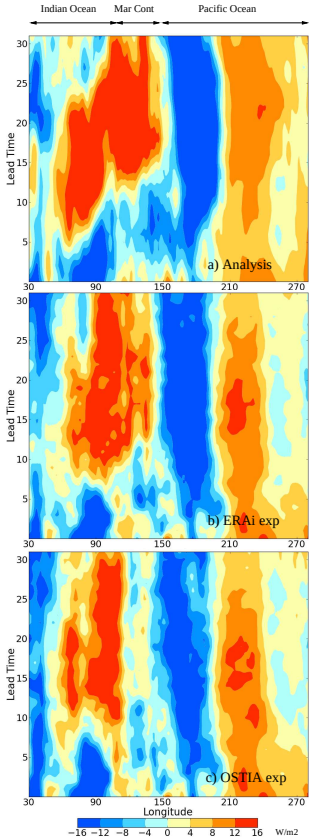

Fig. 3. Longitudinal hovmoller diagrams of the ensemble-mean OLR anomalies (in $W m^{-2}$) averaged between 10° S and 10° N) for starting dates when the convective centre of the MJO is over the Indian Ocean. Negative anomalies indicate active convection while positive anomalies indicate suppressed convection. **(a)** ERA interim analysis, **(b)** ERAi experiment, **(c)** OSTIA experiment.

OSD
9, 2535–2559, 2012

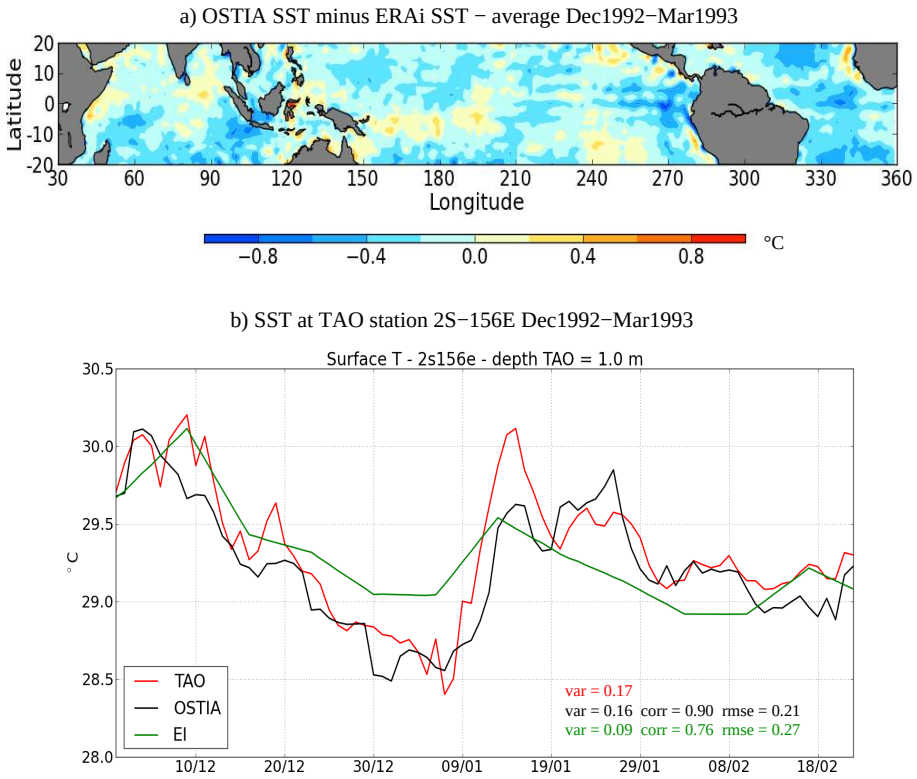

Fig. 4. (a) Difference between OSTIA and ERAi SSTs (in ˚C) averaged over the winter 1992–1993 in the Tropics. **(b)** In-situ SST (temperature observed at 1 m depth, TAO, red line), OSTIA SST (OSTIA, black line), ERAi SST (EI, green line) at the TAO station 2˚ S–156˚ E from December 1992 to March 1993. SST in ˚C. On the background, the variance (var) associated to each SST product is written. For the OSTIA and ERAi SSTs, the correlation (corr) and the root mean square error (rmse) with respect with the TAO SST are also provided.

OSD
9, 2535–2559, 2012

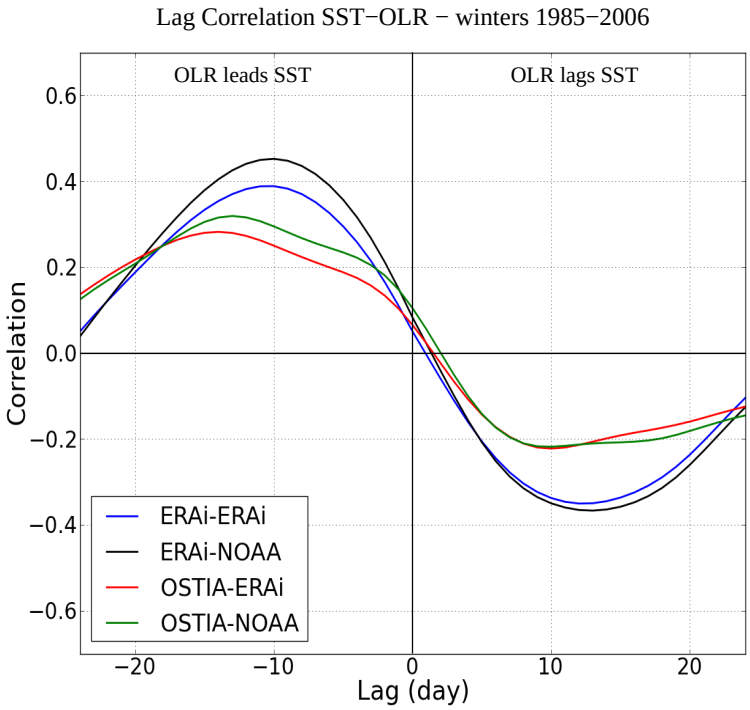

Fig. 5. Lag correlation coefficient between OLR and SST anomalies over the region 5° S–5° N, 60°–95° E over the winters (December–February) 1985–2006 using: SST and OLR from ERA interim (ERAi-ERAi, blue line), ERAi SST and OLR from NOAA (ERAi-NOAA, black line), OSTIA SST and OLR from ERA interim (OSTIA-ERAi, red line) and OSTIA SST and OLR from NOAA (OSTIA-NOAA, green line). The lags are in days. OLR leads SST for negative lags and OLR lags SST for positive lags.

OSD
9, 2535–2559, 2012

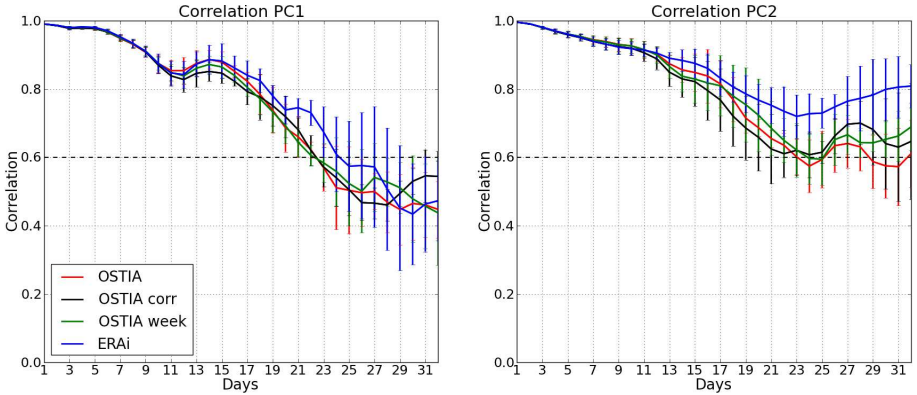

Fig. 6. Same as Fig. 2 for the experiment using OSTIA SST (OSTIA, red line), OSTIA SST with correction of the mean state (OSTIA corr, black line), weekly averaged OSTIA SST (OSTIA week, green line) and ERAi SST (ERAi, blue line).

OSD
9, 2535–2559, 2012

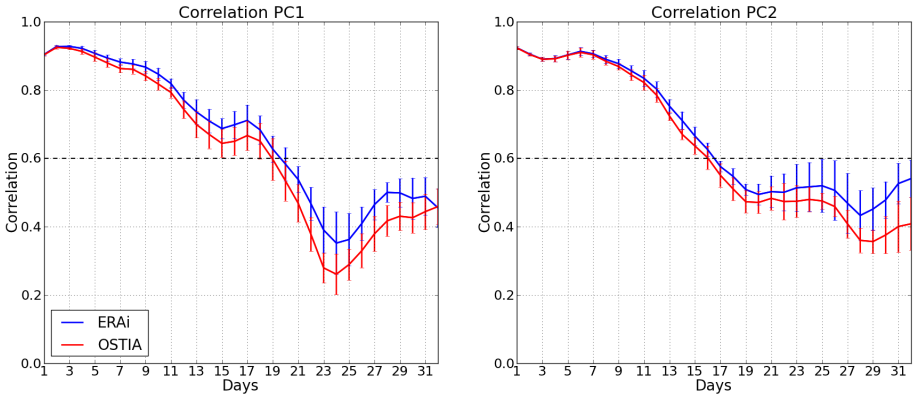

Fig. 7. Same as Fig. 2 for the experiments conducted over 22 winters from 1985 to 2006: ERAi experiment (blue line) and OSTIA experiment (red line).

OSD
9, 2535–2559, 2012

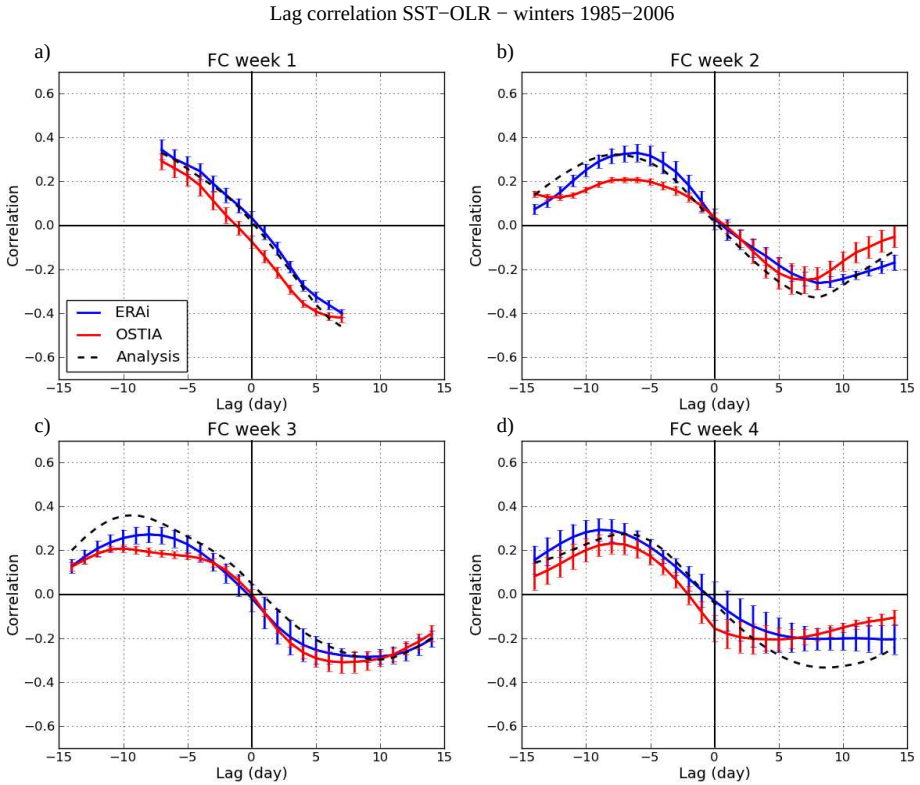

Fig. 8. Lag correlation coefficient between OLR and SST anomalies over the region 5° S–5° N, 60°–95° E averaged according to the forecast week of the experiments conducted over 22 winters (1985–2006): ERAi experiment (blue line) OSTIA experiment (red line) and equivalent in the ERAi reanalysis (black dashed line). **(a)** Week 1, **(b)** 2, **(c)** 3 and **(d)** 4. Error bars stand for the ensemble spread.

OSD
9, 2535–2559, 2012